Planetary Defense Conference 2013
Flagstaff, USA

Session
(please choose one box to be checked)
☐ **1 Planetary Defense – Recent Progress & Plans**
☐ **2 NEO Discovery**
☐ **3 NEO Characterization**
☒ **4 Mitigation Techniques & Missions**
☐ **5 Impact Effects that Inform Warning, Mitigation & Costs**
☐ **6 Consequence Management & Education**

IAA-PDC2013-04-26
Hazardous near Earth asteroid mitigation campaign planning based on uncertain information on fundamental asteroid characteristics

Y. Sugimoto[(1)], G. Radice[(2)], M. Ceriotti[(3)], and J. P. Sanchez[(4)]
[(1)]*University of Glasgow, Glasgow G12 8QQ UK, +44 (0)141 330 8470, y.sugimoto.1@research.gla.ac.uk*
[(2)]*University of Glasgow, Glasgow G12 8QQ UK, +44 (0)141 330 4068, gianmarco.radice@glasgow.ac.uk*
[(3)]*University of Glasgow, Glasgow G12 8QQ UK, +44 (0)141 330 6465, matteo.ceriotti@glasgow.ac.uk*
[(4)]*University of Strathclyde, Glasgow G1 1XQ UK, +44 (0)141 552 5752, jpau.sanchez@strath.ac.uk*

Abstract

Given a limited warning time, an asteroid impact mitigation campaign would hinge on uncertainty-based information consisting of remote observational data of the identified Earth-threatening object, general knowledge on near-Earth asteroids (NEAs), and engineering judgment. Due to these ambiguities, the campaign credibility could be profoundly compromised. It is therefore imperative to comprehensively evaluate the inherent uncertainty in deflection and plan the campaign accordingly to ensure successful mitigation. This research demonstrates dual-deflection mitigation campaigns consisting of primary and secondary deflection missions, where both deflection performance and campaign credibility are taken into consideration. The results of the dual-deflection campaigns show that there are trade-offs between the competing aspects: the total interceptor mass, interception time, deflection distance, and the confidence in deflection. The design approach is found to be useful for multi-deflection campaign planning, allowing us to select the best possible combination of deflection missions from a catalogue of various mitigation campaign options, without compromising the campaign credibility.

1. Introduction

As of today, several asteroid deflection concepts have been proposed and they are under preliminary investigation. Some of these concepts appear to be feasible with the current technology developed through deep space exploration missions, whereas others require certain levels of technological advancement before they can be considered as feasible deflection alternatives. Also, a deflection technique which makes use of nuclear devices for example, involves political issues to be tackled in global cooperation. Nevertheless, we now recognise that it is not unrealistic to prevent an impact event by a modest-sized (<150 metres in diameter) near-Earth asteroid (NEA) if it can be discovered and identified to be threatening about a decade in advance of the impact event [1]. Most importantly, even such small asteroids can cause a local devastation far greater than the Tunguska event in 1908 or the Chelyabinsk meteor event on the 15th of February in 2013. Fortunately, statistically speaking, or based on the NEA population that has been discovered so far, it is more likely that hazardous NEAs to be mitigated will be in this modest size range, rather than kilometre-sized NEAs which can potentially trigger a global catastrophe such as the K-T boundary impact event [2]. This research will therefore focus on hazard mitigation of the modest-sized NEAs with warning times of <10 years.

The most notable feature of asteroid deflection mission is that the characteristics (orbital parameters, physical properties, dynamical properties, etc.) of the NEA are deeply embedded into the design as an integral part of the mitigation systems, and influence their deflection performance. Figure 1 is a schematic diagram that describes

such hazardous asteroid mitigation system design as multidisciplinary system design. The mitigation system design involves three basic vectors **p**, **x**, and **y** where

- **p** is a vector of design parameters representing fundamental properties of the hazardous NEA (e.g. orbit, physical property, etc.) and environmental parameters (e.g. gravity, solar constant, radiation pressure, etc.).

- **x** is a vector of mitigation system design variables (e.g. mass and impact velocity of kinetic impactor (KI), mass of nuclear interceptor (NI), mirror size of solar collector (SC), mass and hovering altitude of gravity tractor (GT), etc.).

- **y** is a vector of mitigation performance indicators of campaign (e.g. total mass of mitigation systems, total interception time, deflection distance, confidence in deflection, etc.).
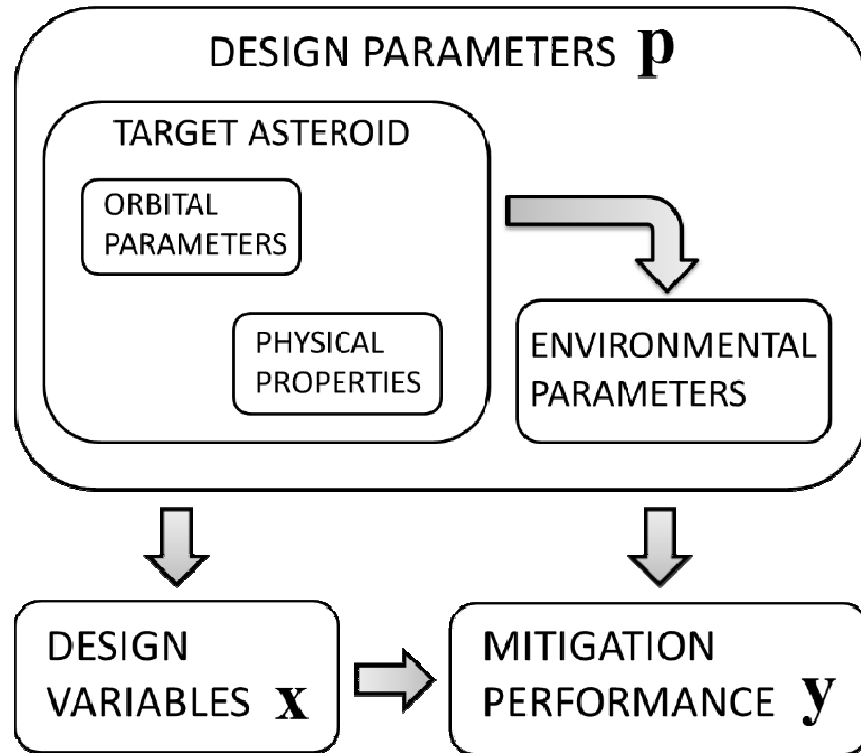

Figure 1 Hazardous NEA mitigation system design.

Recent work by Sugimoto et al. [3] has shown that, for particularly short warning-time impact scenarios (i.e. 10 years), only limited information about the hazardous NEA would be available and that this will most likely come only from ground-based or space-based characterisation approaches. In such cases, the majority of deflection techniques will be subject to epistemic uncertainties and measurement errors in the NEA characteristics, which could lead to compromised outcomes of mitigation. It is therefore essential to investigate mitigation campaign planning that involves design of a reliable and robust hazardous NEA mitigation system. The mitigation campaign should guarantee high confidence in successful mitigation even if the preliminary NEA characterisation is incomplete.

The main objective of this research is to demonstrate a mitigation campaign planning approach that results in efficient, reliable, and yet robust hazardous NEA mitigation for the short warning-time cases. The additional objective is to ensure the flexibility in deflection in order to avoid undesired key-hole passage on the b-plane [4] due to the primary interception.

To fulfil these objectives, we have considered a dual-deflection mitigation approach that makes use of an instantaneous deflection technique (KI) as a primary deflection mission and a slow-push deflection technique (GT) as a secondary deflection mission. The use of a GT as a secondary deflection mission for the secondary impact keyhole avoidance was suggested in the JPL report by Yeomans et al. [5] in 2008. They also pointed out that tracking of the GT spacecraft would provide precise information about the asteroid orbit before and after the primary deflection mission and also after the GT trim manoeuvre. Their study however, assumed the range of the momentum enhancement factor β of the NEA ($1 < \beta < 5$) in order to evaluate possible outcomes of the primary interception achieved through a KI instead of considering the uncertainties in the NEA characteristics. Such combined mitigation measures have been also investigated as a part of the NEOShield project [6].

Design of a dual-deflection mitigation campaign involves trade-offs between the competing aspects (the total interceptor mass, interception time, deflection distance, and the confidence in deflection) which are to be optimised in order to minimise the launch cost of hazardous NEA mitigation systems and total campaign period while maximising the deflection performance and the confidence in successful mitigation campaign.

This paper is articulated as follows. In Section 2, the fundamental aspects of preliminary NEA characterisation subject to warning times and associated epistemic uncertainties, and inevitable measurement errors are briefly highlighted. Section 3 gives an overview on hazardous NEA deflection missions and associated uncertainty in the performance of a given deflection mission due to the incomplete information on the characteristics of the target NEA. Section 4 details the planning of a combined hazardous NEA mitigation campaign consisting of two different deflection missions, followed by optimisation of the initial results. Finally, we present the results of the dual-deflection campaigns consisting of a KI backed up by a GT in Section 5.

2.   Preliminary characterisation of hazardous NEA

Preliminary characterisation of an identified hazardous NEA is essential during the early stages of mitigation campaign planning to appropriately design mitigation systems based on the available information regarding the fundamental characteristics (e.g. physical, dynamical, orbital properties, etc.) of the target NEA. Sending a precursor mission to the NEA is obviously preferable in terms of measurement accuracy as well as to avoid possible mischaracterisation in size, mass, etc.; however, in reality, available characterisation options will be dependent on the given warning time and the NEA orbit.

In the following subsections, three different characterisation approaches – ground-based, space-based, and proximity characterisation – are presented and their degrees of measurement accuracy are briefly summarised. The ground-based characterisation approach is explained more in detail here along with its characterisation diagram as this is the most likely characterisation scenario. Two types of uncertainties – epistemic uncertainties and measurement errors – associated with the preliminary NEA characterisation are then introduced. In addition, aleatory uncertainties are presented for reference, since these are related to the practical limitations (i.e. errors) on mitigation systems (e.g. lack of precision).

2.1.   Characterisation scenarios

Depending on the available warning time, preliminary characterisation of a hazardous NEA will vary since each characterisation approach will have a different degree of uncertainty. There are basically three different preliminary characterisation approaches: ground-based, space-based, and proximity characterisation.

The ground-based characterisation makes use of telescopic and radar observations from the Earth whereas the space-based characterisation leverages infrared astronomical satellites (IRAS) in space in addition to the ground-based observation options. These two characterisation scenarios would require only a few days during close Earth approaches of NEAs to complete the preliminary characterisation [7], which means they could be possibly used simultaneously with the first discovery of a hazardous NEA by radar or telescope. On the other hand, the proximity characterisation approach, which requires a precursor mission to the target NEA, would take <1¼ years to complete the preliminary characterisation [8]. The availability of precursor mission is subject to the orbit of an identified threatening NEA while, particularly for the short warning-time cases, quick preliminary characterisation is essential to ensure a wider mitigation campaign window (i.e. the period between the Earth departure of mitigation systems and the completion of NEA interception). The wider campaign window results in more mitigation campaign options and more efficient mitigation, even though the preliminary characterisation may remain incomplete without a precursor mission.

The accuracy of observational information by the ground-based characterisation is based on the capability of ground-based telescopes and radar instruments on Earth, and thus the majority of physical parameters of the target object will remain highly uncertain [9]. Microscopic properties of a NEA can be estimated by analysing the surface colour and solar spectral reflectance while macroscopic characteristics such as the mass and the porosity are much more difficult to be ascertained particularly when the object is only a few hundred metres or so in diameter. According to Müller et al. [10], the ground-based telescopic observations with the state-of-art mid-infrared module (TIMM-2) have demonstrated higher performance at NEA characterisation than the radar telescopic observations (e.g. Arecibo and Goldstone) as the asteroid sub-surface/internal structures can be roughly estimated through thermal characterisation of the asteroidal surface. However, in this study, such advanced ground-based mid-infrared observations are not considered to distinguish the ground-based characterisation from the space-based characterisation which makes use of infrared observation.

Figure 2 is the simplified diagram of the ground-based characterisation approach. The fundamental physical characteristics (mass, size, albedo, and momentum enhancement) for mitigation system design are derived from the ground-based observational data, meteorite analogues of the NEA, and expert opinions regarding the macro porosity (i.e. large structural flaws inside the NEA). Crucially, the mass determination of the NEA cannot be done directly through the ground-based observations since it requires additional information from meteorite analogues regarding the microscopic characteristics of the main material that composes the asteroid and expert opinions

regarding the macro porosity to estimate the bulk density of the NEA. It is therefore inevitable that there would be major uncertainties in the preliminary characterisation, particularly in the mass (i.e. bulk density) and albedo value for the case of ground-based characterisation.
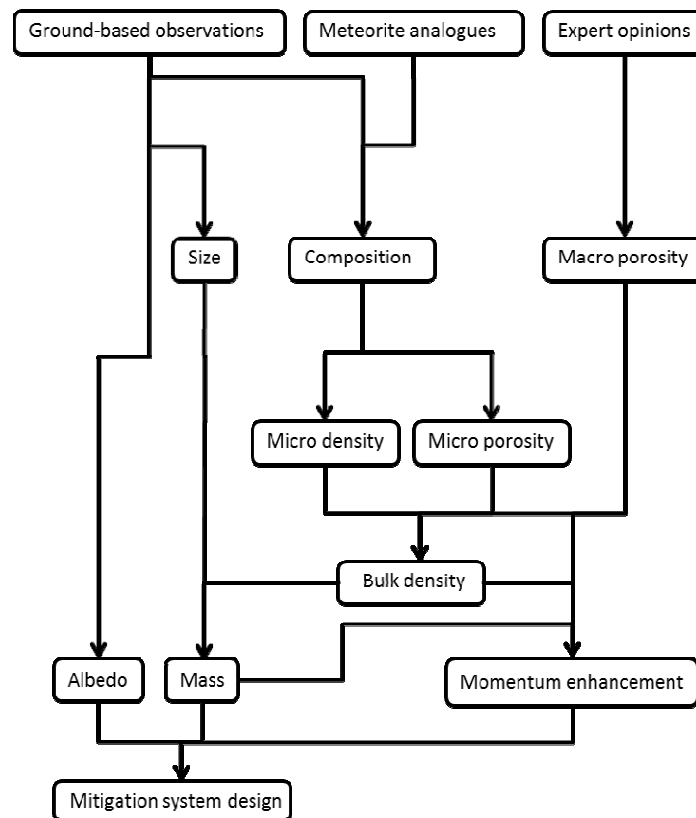

Figure 2 Ground-based characterisation diagram.

2.2.   Types of uncertainty

There are three basic types of uncertainty – epistemic uncertainty, error (i.e. numerical uncertainty), and aleatory uncertainty – derived from different sources regarding the NEA characteristics or mitigation systems.

In general, epistemic uncertainties arise when a system is not sufficiently characterised, certain characteristics of the system are neglected, or the physical model of the system is based on hypotheses rather than experiments. Our current characterisation on the NEA population including potentially hazardous asteroids is insufficient, hence epistemic uncertainties exist in general knowledge on NEAs. This type of uncertainties can be reduced by obtaining more credible information on the specific threatening NEAs or by improving general knowledge on the NEA population. Moreover, epistemic uncertainties also exist in design of low Technology Readiness Level (TRL) components of a mitigation system such as the solar-pumped laser ablation system [11]. Unlike aleatory uncertainties, representation of epistemic uncertainties requires an appropriate quantification technique such as Evidence Theory [12].

Errors (i.e. numerical uncertainties) are a recognisable deficiency due to practical constraints on a system in general. The in-situ mass determination by the Hayabusa spacecraft, for example, had about 5% of measurement error which is thought to be due to the relatively small mass of Itokawa [13] – 190,000 times smaller than that of Eros, whose mass was determined within 0.05% [14]. The size determination of NEAs from the ground is also subject to the resolution of telescopic and radar images due to the practical constraints on the ground-based observational instruments. This type of uncertainties can be minimised by simply applying more accurate measurement techniques. Unlike the other types of uncertainties, the source is often known such that one can often estimate error magnitudes in advance. Measurement errors in NEA size, rotation state, and shape determination could be as significant as epistemic uncertainties in mass determination, however the hazardous asteroid is modelled as a spherical body throughout this work and these problems are not dealt with.

Aleatory uncertainties (also known as inherent uncertainties) represent a random variation in a system, which is inevitably present in every outcome of the system. For the case of KI, there will be, for instance, a certain amount of possibility of missing the target point on the NEA surface, or at worst the NEA itself due to aleatory uncertainties in the precision of the KI system. Such practical limitations of the KI technique is associated with epistemic uncertainties and measurement errors in NEA size, rotation state, shape, centre of gravity, etc., and a very high-speed impact (10–20 km/s) relative to a modest-sized object in space. For the case of SC, the acceleration of the target body (i.e. the surface material evaporation rate) will always fluctuate due to aleatory

uncertainties in the solar flux, the asteroid surface condition, the mirror degradation with time. This type of uncertainties cannot be completely eliminated but they can be mathematically modelled using a conventional probability theory, once a sufficient amount of statistical data is available. However, such aleatory uncertainties in deflection techniques are not considered in this work.

Epistemic uncertainties will be the most common cause of the uncertain physical properties of the target body, followed by measurement errors unless our general knowledge on NEAs is abundant and non-biased. Table 1 summarises the uncertainties in NEA mass M_a and geometric albedo p_v corresponding to the three different characterisation options and three different taxonomic classes: S-type, C-type, and M-type, where the NEA mass M_a can be determined by referring to the micro density ρ_{micro}, bulk porosity P_{bulk}, and the equivalent diameter d of the NEA, according to Equation (1).

$$M_a = \rho_{micro}(1 - P_{bulk}) \times 4\pi(d/2)^3/3 \tag{1}$$

These uncertainties originate from the lower and upper bounds of the uncertain NEA physical properties given in Table 10 in Appendix A.1. As can be seen, more rigorous but possibly more time-consuming characterisation results in smaller ranges of uncertainties in the physical properties for all the taxonomic classes. Interested readers should refer to Appendices A.1 for further details on the uncertain NEA physical properties.

Table 1 Uncertainties in the mass M_a and the geometric albedo p_v of the NEA corresponding to the ground-based, space-based, and the proximity characterisation scenarios. They are represented in percentage relative to the mean physical properties of each taxonomic class. A) S-type. B) C-type. C) M-type.

A)	Ground-based	Space-based	Proximity
M_a	-36.1–45.7%	-28.8–36.8%	-5.4–9.0%
p_v	-46.4–50.0%	-23.8–31.7%	-10.0–10.0%

B)	Ground-based	Space-based	Proximity
M_a	-41.3–45.6%	-32.3–35.5%	-4.0–4.7%
p_v	-26.5–34.1%	-23.8–31.7%	-10.0–10.0%

C)	Ground-based	Space-based	Proximity
M_a	-27.3–24.5%	-21.5–20.8%	-3.0–2.0%
p_v	-28.6–42.9%	-23.8–31.7%	-10.0–10.0%

3. Hazardous NEA deflection

The deflection representation of hazardous NEAs in this work is based on the b-plane concept that is applied to planetary encounter analyses [4]. The b-plane is oriented normal to the incoming asymptote of the osculating geocentric hyperbola, in other words, it is oriented normal to the object's unperturbed geocentric velocity vector $\mathbf{U}_{NEA}|_{nominal}$ as shown in Figure 3-A). The b-plane analysis can not only determine whether an Earth collision is possible, but also determine how close to Earth the encounter will be. Furthermore, understanding the position of an Earth encountering object on the b-plane (i.e. the uncertainty ellipsoid projected on the b-plane) is prerequisite to the keyhole analysis. The minimum distance of the unperturbed trajectory at the closest approach point on the b-plane is called the impact parameter b denoted by a red line segment in Figure 3-B). The impact parameter itself does not reveal whether the perturbed trajectory will intersect the Earth sphere; however, it can be available by scaling Earth's radius $r_\oplus$ according to Equation (2)

$$b_\oplus = r_\oplus\sqrt{1 + v_e^2/v_\infty^2} \tag{2}$$

where v_e is Earth's escape velocity and v_∞ is the hyperbolic excess velocity given as follows.

$$v_e^2 = 2GM_\oplus/r_\oplus \tag{3}$$

$$v_\infty^2 = \mu_\odot\left(3 - 1/a - 2\sqrt{a(1 - e^2)}\cos i\right) \tag{4}$$

A given trajectory intersects the Earth sphere if b is smaller than the scaled Earth-radius $b_\oplus$, and not otherwise. On the b-plane the ξ coordinate is the minimum distance that can be obtained by varying the timing of the encounter. This distance, known as the minimum orbital intersection distance (MOID), is equivalent to the minimum separation between the osculating ellipses, regardless of the location of the objects on their orbits. Throughout this work, the MOID between Earth and a NEA is set to zero and the Earth is located right at the origin of the geocentric coordinate system $(\xi,\ \eta,\ \zeta)$ on the b-plane as shown in Figure 3-A).
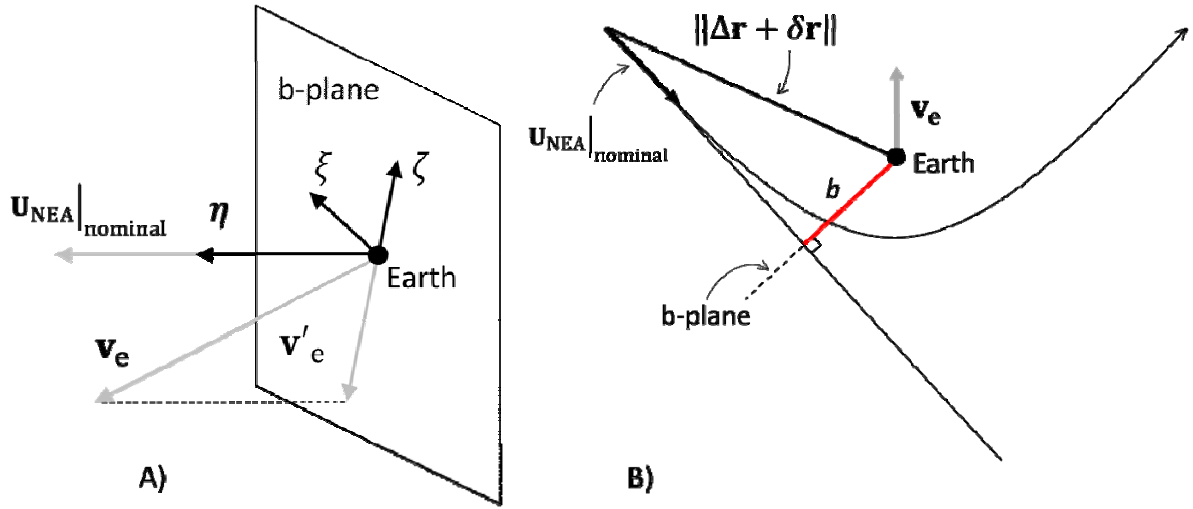
Figure 3 A) Geocentric coordinate system $(\xi,\ \eta,\ \zeta)$ on a b-plane. B) Geometry of hyperbolic passage.

A hazardous NEA mitigation campaign therefore comes down to nudging the NEA and making b at least greater than $b_\oplus$ on the b-plane of the impact epoch. Achieved deflections on the b-plane by the instantaneous and slow-push deflection techniques are computed by solving the proximal motion equations and Gauss' variational equations [15].

Two instantaneous deflection techniques (KI and NI) and two slow-push deflection techniques (SC and GT) are considered here. The mathematical models of these techniques are basically based on the models used in the work of Sugimoto et al. [3], which are originally developed in the work of Sanchez et al. in 2009 [1].

In the next subsections, six virtual hazardous NEAs to be mitigated and the associated hazard scenario are presented and the objective of NEA deflection on the b-plane is summarised. Finally, the derivation method and algorithm to represent the uncertainties in NEA deflection by Evidence Theory are introduced.

3.1.   Virtual hazardous NEAs

Virtual Earth-threatening impactors are imaginary hazardous asteroids on collision courses with Earth that will be intercepted by mitigation campaigns in this study. Six virtual impactors (VI_1–VI_6) were generated to represent a realistic population of impactors by taking into account the relative impact frequency of each possible trajectory [16]. The impact frequency of each trajectory was estimated by means of Öpik's collision theory [17] and Bottke's near-Earth objects orbital model [18]. The orbits of the virtual Earth impactors are shown in Figure 4. The orbit type of VI_1, VI_2, VI_4, and VI_6 is Apollo whereas that of VI_3 and VI_5 is Aten. The Keplerian elements of the virtual impactors are given in Table 2.

The equivalent diameter of the virtual impactors is 140 metres unless otherwise stated. This is due to the fact that NEAs with 140 metres in diameter would represent more or less the worst possible size among the subkilometre-sized NEA population in the foreseeable future. These relatively small NEAs can cause serious local-scale devastation on Earth and yet are not sufficiently discovered through the previous near-Earth object (NEO) surveys (e.g. the George E. Brown, Jr. Near-Earth Object Survey section of the 2005 NASA Authorization Mission, etc.). The B612 Foundation's Sentinel mission may detect 90% of NEOs 140 metres in diameter or greater by 2020 and a fraction of those smaller than 140 metres [19], however detection of <140-metre sized NEOs will not likely reach a 90% discovery rate, at least in the next decade to come.

The Earth impact events of the virtual impactors take place on the 13th of April 2036 while each impactor is discovered and identified to be truly hazardous 10 years before the impact event, and thus a mitigation campaign will be launched and executed sometime in this 10-year warning time (i.e. between 2026/4/13 and 2036/4/13). Although there is only <20% chance that a >200-metre sized NEA would be discovered before the Earth impact given the capability of current telescopic surveillance according to the work by Morrison et al. [20], this warning time is assumed to be a reasonable period of time for 140-metre sized NEAs.
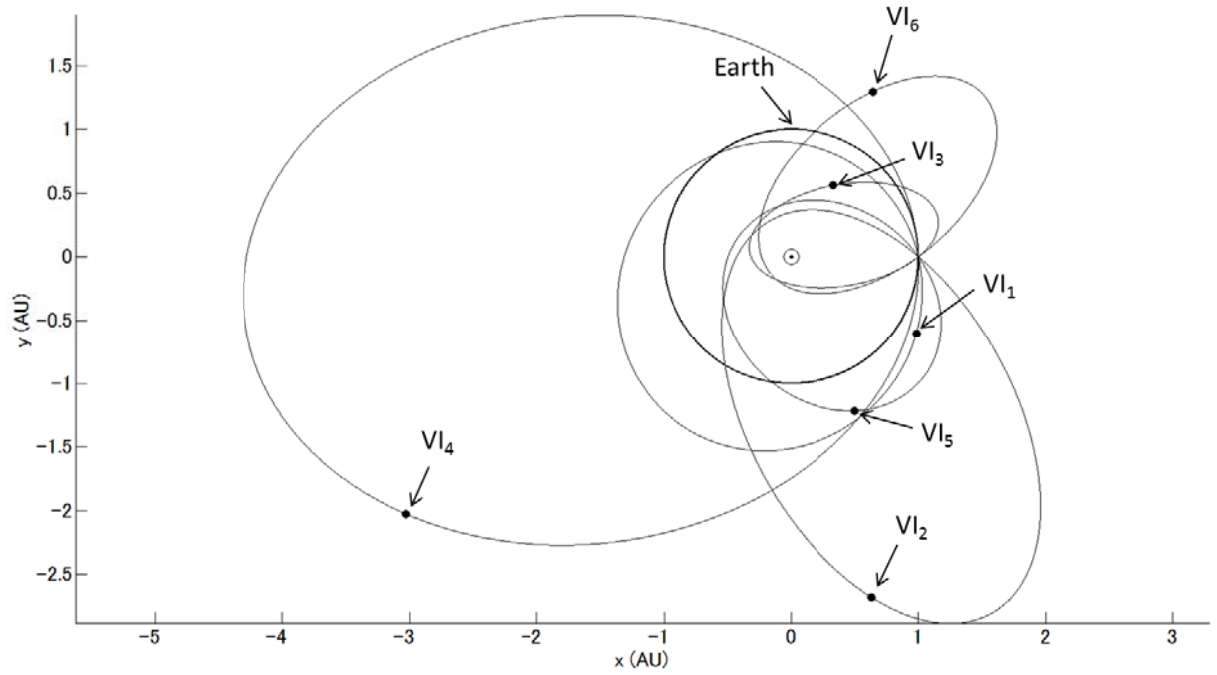
Figure 4 Orbits of the virtual impactors and Earth on the ecliptic plane.

Table 2 Keplerian elements of the virtual impactors. θ_{MOID} represents the true anomaly at the MOID point.

	a (AU)	e	i (deg)	Ω (deg)	ω (deg)	θ_{MOID} (deg)
VI_1	1.24	0.289	7.5	180	242	298
VI_2	1.78	0.813	2.5	0	119	241
VI_3	0.80	0.627	52.5	0	214	146
VI_4	2.66	0.625	2.5	180	186	354
VI_5	0.95	0.550	22.5	180	308	233
VI_6	1.10	0.808	7.5	0	220	140

3.2. Objective of NEA deflection on b-plane

There are two kinds of deflection distances to be considered – the minimum required deflection distance and the safe deflection distance. The minimum required deflection distance is simply equivalent to $b_\oplus$ whereas the safe deflection distance is set to $b_{\mathrm{safe}} = 2.5$ Earth-radii throughout this work. The latter is thought to be a desired deflection distance to safely avoid an asteroid impact with Earth by the Committee to Review Near-Earth Object Surveys and Hazard Mitigation Strategies; National Research Council [2].

The objective of hazardous NEA deflection mission is therefore to make the impact parameter b on the 2036 b-plane at least greater than $b_\oplus$, or b_{safe} if possible. Table 3 shows $b_\oplus$, b_{safe}, required impulsive velocity changes $\Delta v_\oplus$ to achieve $b_\oplus$, and required impulsive velocity changes Δv_{safe} to achieve b_{safe} for the mitigation of $VI_{1\text{-}6}$, respectively. These required impulsive velocity changes are computed for the optimal interception epochs (i.e. perihelia of $VI_{1\text{-}6}$) when a required velocity change is minimised, given the 10-year warning time.

Table 3 Minimum deflection distance $b_\oplus$, safe deflection distance b_{safe}, impulsive velocity change $\Delta v_\oplus$, and the impulsive velocity change Δv_{safe} that are required for the mitigation of $VI_{1\text{-}6}$. The optimal interception epochs for respective virtual impactors range 2026/10/9–2027/8/14.

	$b_\oplus$ (Earth-radius)	b_{safe} (Earth-radius)	$\Delta v_\oplus$ (cm/s)	Δv_{safe} (cm/s)	Interception Epoch
VI_1	1.664	2.5	0.792	1.192	2026/10/9
VI_2	1.077	2.5	0.191	0.443	2026/12/10
VI_3	1.076	2.5	0.529	1.229	2026/11/21
VI_4	1.661	2.5	1.375	2.069	2027/8/14
VI_5	1.148	2.5	0.495	1.077	2027/2/17
VI_6	1.078	2.5	0.271	0.627	2026/12/23

3.3. Uncertainty in NEA deflection

In this subsection, the performance of deflection techniques subject to epistemic uncertainties in the physical properties of the hazardous NEA is evaluated, where Evidence Theory [12] is employed to quantify the uncertainty in deflection performance. KI, NI, SC, and GT are applied to VI_{1-6} of different taxonomic classifications (S-, C-, and M-types) at different characterisation levels (ground-based, space-based, and proximity characterisation) for reference.

Evidence Theory makes use of two probability measures called Belief (Bel) and Plausibility (Pl) as illustrated in Figure 5. Belief represents confidence in the truth of an event $\mathcal{A}$ (i.e. deflection) exclusive of uncertainty while Plausibility represents confidence in the truth of the same event inclusive of uncertainty.
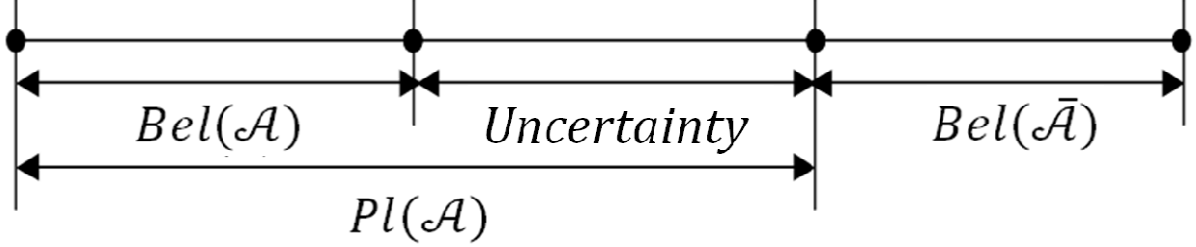

Figure 5 Belief and Plausibility [21].

Unlike probability measures of conventional probabilistic means, the sum of the Belief measure of the truth of the event $\mathcal{A}$ and that of its negation is not necessarily unity as seen in Equation (5).

$$Bel(\mathcal{A}) + Bel(\bar{\mathcal{A}}) \neq 1 \tag{5}$$

The two probability measures are therefore subject to the uncertain NEA characteristics in different ways; however, the more rigorous the preliminary characterisation is, the less different the two measures will be. Belief informs the lower bounds of deflection outcomes whereas Plausibility informs the upper bounds of deflection outcomes. To this extent, Belief is found to be useful for more strict assessment of confidence level on deflection missions.

In order to evaluate Belief and Plausibility of a given deflection, basic probability assignment (BPA) structures for the NEA physical properties must be assembled (see Appendix A.1 for further details). A BPA $m(\mathcal{E})$ is a basic uncertainty measure which represents the degree of confidence in the truth of an event $\mathcal{E}$ (i.e. specific NEA physical property) and satisfies the following three axioms:

$$m(\mathcal{E}) \geq 0 \text{ for any } \mathcal{E} \in 2^{\mathcal{U}} \tag{6}$$

$$m(\emptyset) = 0 \tag{7}$$

$$\sum m(\mathcal{E}) = 1 \text{ for all } \mathcal{E} \in 2^{\mathcal{U}} \tag{8}$$

where $\emptyset$ denotes an empty set. All the events $\mathcal{E}$ that are subsets of the universal set $\mathcal{U}$ ($\mathcal{E} \subseteq \mathcal{U}$) and those which have $m(\mathcal{E}) > 0$ are known as the focal elements.

Epistemic uncertainties and parametric uncertainties (i.e. measurement errors) in a given parameter are described as a set of intervals with associated BPAs. Figure 6 is a schematic representation of such a BPA structure for the uncertain parameter p_1. In Table 4, the intervals for p_1 are non-nested with each other, however in general, they can be nested. These interval values are usually obtained from observations and experiments as well as from expert opinions and hypotheses (see Appendix A.1 for further details).
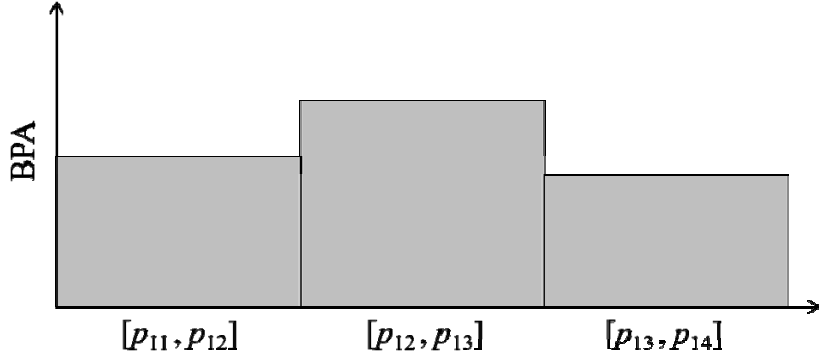
Figure 6 BPA structure for the uncertain parameter p_1.

Table 4 Intervals with associated BPAs for the uncertain parameter p_1.

Uncertain parameter	Interval	BPA
p_1	$[p_{11}, p_{12}]$	m_{11}
	$[p_{12}, p_{13}]$	m_{12}
	$[p_{13}, p_{14}]$	m_{13}

Evidence-based information from different sources that supports the truth of an event $\mathcal{A}$ can be aggregated using existing rules of combination. In this study, the Dempster rule of combination [21] given in Equation (9) is used, where $m_1(\mathcal{B})$ and $m_2(\mathcal{C})$ are the degrees of confidence in the truth of an event $\mathcal{B}$ and that in the truth of an event $\mathcal{C}$, respectively.

$$m(\mathcal{A}) = \frac{\sum_{\mathcal{B} \cap \mathcal{C} = \mathcal{A}} m_1(\mathcal{B}) m_2(\mathcal{C})}{1 - \sum_{\mathcal{B} \cap \mathcal{C} \neq \emptyset} m_1(\mathcal{B}) m_2(\mathcal{C})} \quad , \mathcal{A} \neq \emptyset \tag{9}$$

Belief is then computed by summing the BPAs of events $\mathcal{B}$ that totally support the truth of the event $\mathcal{A}$ while Plausibility is computed by summing the BPAs of events $\mathcal{B}$ which totally or partly support the truth of the event $\mathcal{A}$ as shown Equation (10) and Equation (11), respectively. In other words, Belief and Plausibility inform the lower and upper bounds of the event $\mathcal{A}$ respectively. They pertain to each other by Equation (12).

$$Bel(\mathcal{A}) = \sum_{\mathcal{B}|\mathcal{B} \subseteq \mathcal{A}} m(\mathcal{B}) \tag{10}$$

$$Pl(\mathcal{A}) = \sum_{\mathcal{B}|\mathcal{B} \cap \mathcal{A} \neq \emptyset} m(\mathcal{B}) \tag{11}$$

$$Pl(\mathcal{A}) + Bel(\bar{\mathcal{A}}) = 1 \tag{12}$$

In this work, the following steps are performed to evaluate Belief and Plausibility of asteroid deflection:

a) Collect all the necessary information on the asteroid characteristics from different literature (see Appendix A.1 for further details on information gathering).
b) Determine the nominal physical properties (i.e. mean values) of the NEA from the information collected in step a) as shown in Table 5, and design a mitigation system based on this baseline for the nominal deflection distance b_{nom} within $b_{\oplus} < b_{nom} < b_{safe}$ (b_{nom} is a deflection distance on the b-plane that will be achieved through the given deflection mission to the NEA with the nominal physical properties.).
c) Assemble BPA structures for the NEA characteristics by forming each uncertainty parameter as a set of intervals with the prescribed BPAs and, if necessary, integrate BPA structures of the same parameter from different sources by using the Dempster rule of combination given by Equation (9) (BPA structures are provided in Table 10 in Appendix A.1.).
d) Calculate a set of intervals of the NEA mass M_a and momentum enhancement factor β with associated BPAs (The BPA for each interval is simply the product of BPAs of related physical properties that support the truth of that interval).
e) Given the mitigation system designed in step b) and the BPA structures for M_a and β from step d), compute a set of intervals of all the possible deflection b with associated BPAs.
f) Computed Belief $Bel(b)$ and Plausibility $Pl(b)$ in an arbitrary deflection b by Equation (13) and (14) where set C_i consists of a set of intervals of deflection b with associated BPA $m_c(C_i)$.

$$Bel(b) = \sum_{C_i|C_i \subseteq b} m_c(C_i) \tag{13}$$

$$Pl(b) = \sum_{C_i|C_i \cap b \neq \emptyset} m_c(C_i) \tag{14}$$

Table 6 shows an example of BPA structures for the NEA mass M_a, momentum enhancement factor β, deflection b on the 2036 b-plane, and impulsive velocity change Δv given by KI. In this case, the nominal deflection b_{nom} is set to 2.5 Earth-radii and the target NEA is VI$_1$ of S-type characterised at the ground-based level. M_a can be calculated simply by Equation (1) whereas β is obtained by a solution of Equation (15) originating from the work by Holsapple et al. [22].

$$\beta = 1 + (0.083)U^{0.2}Y^{-0.1}\rho_{\text{bulk}}^{-0.1}\delta^{0.2} \tag{15}$$

where U is impactor velocity, Y is the material strength of the target asteroid, and δ is the impactor density. The material strength of S-type is assumed to be 10 kPa and the impactor density is set to 3.0 g/cm^3. The bulk density is given by $\rho_{\text{bulk}} = \rho_{\text{micro}}(1 - P_{\text{bulk}})$. The impactor velocity for the case of KI is one of the design variables, hence is simply subject to the mitigation system design.

Table 5 Nominal physical properties of three asteroid classes; micro density ρ_{micro}, micro porosity P_{micro}, bulk density ρ_{bulk}, bulk porosity P_{bulk}, geometric albedo p_v, and NEA mass M_a. A) Ground-based characterisation scenario. B) Space-based characterisation scenario. C) Proximity characterisation scenario. The mitigation system is designed based on the nominal physical properties instead of considering a system margin approach or the worst NEA characteristics.

A)	ρ_{micro} (g/cm^3)	P_{micro} (%)	ρ_{bulk} (g/cm^3)	P_{bulk} (%)	p_v	M_a (kg)
S-type	3.45	10.66	2.20	36.17	0.19	3.17×10^9
C-type	2.71	23.00	2.21	47.36	0.05	2.05×10^9
M-type	7.87	0.60	2.27	17.55	0.12	9.32×10^9

B)	ρ_{micro} (g/cm^3)	P_{micro} (%)	ρ_{bulk} (g/cm^3)	P_{bulk} (%)	p_v	M_a (kg)
S-type	3.45	10.66	1.42	36.12	0.18	3.17×10^9
C-type	2.71	23.00	1.43	47.34	0.05	2.05×10^9
M-type	7.87	0.60	1.47	17.45	0.12	9.33×10^9

C)	ρ_{micro} (g/cm^3)	P_{micro} (%)	ρ_{bulk} (g/cm^3)	P_{bulk} (%)	p_v	M_a (kg)
S-type	3.45	10.89	6.49	34.35	0.19	3.26×10^9
C-type	2.70	23.00	6.49	45.71	0.05	2.11×10^9
M-type	7.88	0.60	6.85	13.14	0.12	9.84×10^9

Table 6 Example of BPA structures for NEA mass M_a, momentum enhancement factor β, deflection b on the 2036 b-plane, and the impulsive velocity change Δv by KI with impact velocity of 16.4 km/s. b_{nom} is set to 2.5 Earth-radii and the target NEA is VI$_1$ of S-type characterised at the ground-based level.

	M_a (kg)		β		b (Earth-radius)		Δv (cm/s)		$m_c(C_i)$
	Lower bound	Upper bound	Lower bound	Upper bound	Lower bound	Upper bound	Lower bound	Upper bound	
C_1	2.02×10^9	2.37×10^9	1.55	1.54	3.33	3.93	2.33	2.75	0.04
C_2	2.07×10^9	2.51×10^9	1.55	1.54	3.14	3.84	2.20	2.69	0.04
C_3	2.19×10^9	2.66×10^9	1.55	1.54	2.96	3.62	2.07	2.53	0.05
C_4	2.32×10^9	2.76×10^9	1.55	1.54	2.85	3.41	1.99	2.39	0.01
C_5	2.32×10^9	2.85×10^9	1.55	1.53	2.76	3.41	1.93	2.39	0.09
C_6	2.37×10^9	3.02×10^9	1.54	1.53	2.60	3.33	1.82	2.33	0.08
C_7	2.51×10^9	3.19×10^9	1.54	1.53	2.45	3.14	1.72	2.20	0.09
C_8	2.66×10^9	3.31×10^9	1.54	1.53	2.36	2.96	1.65	2.07	0.02
C_9	2.78×10^9	3.32×10^9	1.54	1.53	2.35	2.82	1.65	1.98	0.04
C_{10}	2.85×10^9	3.52×10^9	1.53	1.52	2.21	2.76	1.55	1.93	0.04
C_{11}	3.02×10^9	3.72×10^9	1.53	1.52	2.09	2.60	1.46	1.82	0.05
C_{12}	3.19×10^9	3.86×10^9	1.53	1.52	2.01	2.45	1.41	1.72	0.01
C_{13}	3.25×10^9	3.96×10^9	1.53	1.52	1.96	2.41	1.37	1.68	0.13
C_{14}	3.32×10^9	4.20×10^9	1.53	1.51	1.84	2.35	1.29	1.65	0.12
C_{15}	3.52×10^9	4.44×10^9	1.52	1.51	1.74	2.21	1.22	1.55	0.14
C_{16}	3.72×10^9	4.61×10^9	1.52	1.51	1.68	2.09	1.17	1.46	0.03

The results for the uncertainties in the outcomes (i.e. deflection distance b) of respective deflection techniques represented by the Belief and Plausibility measures are shown in Figure 7, Figure 8, and summarised in Table 7. Firstly, it can be seen that Belief and Plausibility measures inform lower and upper bounds of the outcomes of deflection missions. Such straightfoward information is available through a conventional system margin approach which only considers a series of possible ranges of system design parameters (e.g. M_a and β) without assigning probabilities (i.e. outcomes of interception are always given as a plain interval value without carrying any information about epistemic uncertainties within the interval.). On the other hand, these probability measures associated with Evidence Theory indicate confidence in every possible outcome of deflection missions, which is directly related to the source of uncertainty and current uncertainty level. To this extent, Evidence Theory allows a more rigorous quantification of uncertainties than the aforementioned system margin approach does.

The results indicate that no matter how much literature or how many expert opinions one refers to for mitigation system design, as long as there are epistemic uncertainties and measurement errors in observational data, the uncertainty in deflection will be present. In other words, for whatever deflection b with $Bel(b) < 1.0$, the confidence in achieving that deflection distance is to a greater or lesser extent, compromised.

Depending on the physical properties that are related to each deflection technique and also the taxonomic class of the asteroid, Belief/Plausibility of the deflection varies. Due to the substantial amount of uncertainty in albedo shown in Table 1, the performance of the SC is fairly compromsied as seen in Figure 8-C) whereas Figure 7-A) and Figure 7-B) indicate that the KI and the NI are subject to more or less the same amount of uncertainty. This can be interpred as both KI and NI are instantaneous deflection techniques that are equally dependent on the uncertainties in the mass and the momentum multiplication of the NEA but independent of the albedo value.

Figure 8-D) shows a series of results for the GT, where the amount of uncertainty in deflection is clearly smallest among the four deflection techniques in any characterisation scenarios as well as for any types of asteroid. These results indicate that the performance of GT is least dependent on the epistemic uncertainties in NEA physical characteristics, particularly on the uncertainty in mass. The remarkable aspect of the GT technique is that the performance of GT is a function of the NEA mass because the technique simply makes use of the gravitational pull between the asteroid and the GT spacecraft; the heavier/lighter the asteorid mass is, the larger/smaller the gravitational pull will be. This is remarkable considering the fact that the GT is the least efficient deflection technique among the ones being evaluated, in terms of both yield-to-weight and interception period. To this extent, a GT would be suitable for a secondary interceptor that backs up a more unpredictable but efficient instantaneous deflection attept.

In summary, unless the preliminary characterisation is conducted at the proximity characterisation level, the outcome of a NEA deflection mission will always lack precision, whatever the design parameters (e.g. nominal NEA characteristics) and the design variables (e.g. interceptor mass, impact velocity, mirror size, etc.) are selected, hence the deflection performance will be compromised. Considering a system margin (i.e. increasing the deflection performance of a single mitigation system) in order to ensure $Bel(b_{\mathrm{safe}}) = 1.0$ is valid here, however the aim of this work is not to design a single mitigation system that is capable of providing a desired deflection at its worst possible performance but to develop a mitigation campaign consisting of multi-deflection mission that retains a certain level of confidence in achieving a desired deflection even if the primary deflection mission is unsuccesful.

Table 7 Lower and upper bounds of the deflection b (Earth-radius) on the 2036 b-plane for different deflection techniques, characterisation scenarios, and taxonomic classes. A) KI. B) NI. C) SC. D) GT.

A)	S-type	C-type	M-type
Ground-based	1.70–3.97	1.70–4.38	2.05–3.33
Space-based	1.81–3.55	1.83–3.75	2.11–3.11
Proximity	2.29–2.66	2.38–2.61	2.45–2.57

B)	S-type	C-type	M-type
Ground-based	1.71–3.93	1.71–4.32	2.01–3.33
Space-based	1.82–3.52	1.84–3.71	2.11–3.12
Proximity	2.29–2.65	2.34–2.62	2.46–2.57

C)	S-type	C-type	M-type
Ground-based	1.11–5.23	1.60–4.60	1.46–4.54
Space-based	1.34–4.23	1.74–3.90	1.61–3.99
Proximity	2.15–2.85	2.35–2.63	2.35–2.74

D)	S-type	C-type	M-type
Ground-based	2.32–2.81	2.38–2.85	2.25–2.86
Space-based	2.35–2.79	2.41–2.80	2.29–2.77
Proximity	2.48–2.56	2.49–2.54	2.48–2.54

Figure 7 Belief and Plausibility of deflection on the 2036 b-plane for different characterisation scenarios and asteroid classes. Black lines represent Belief measures whereas dashed black lines represent Plausibility measures. Green lines represent the nominal deflection distance b_{nom}. A) KI. B) NI.
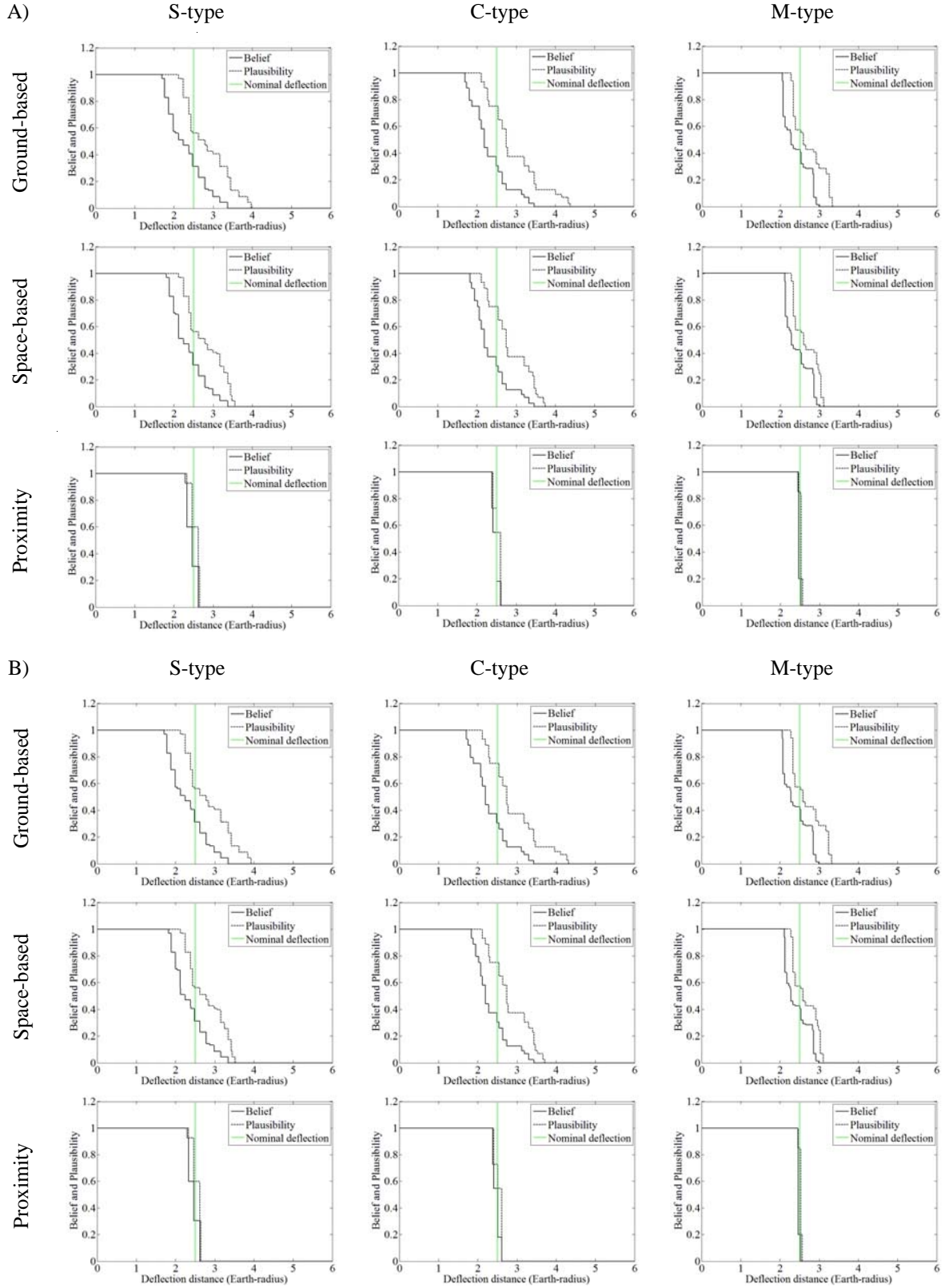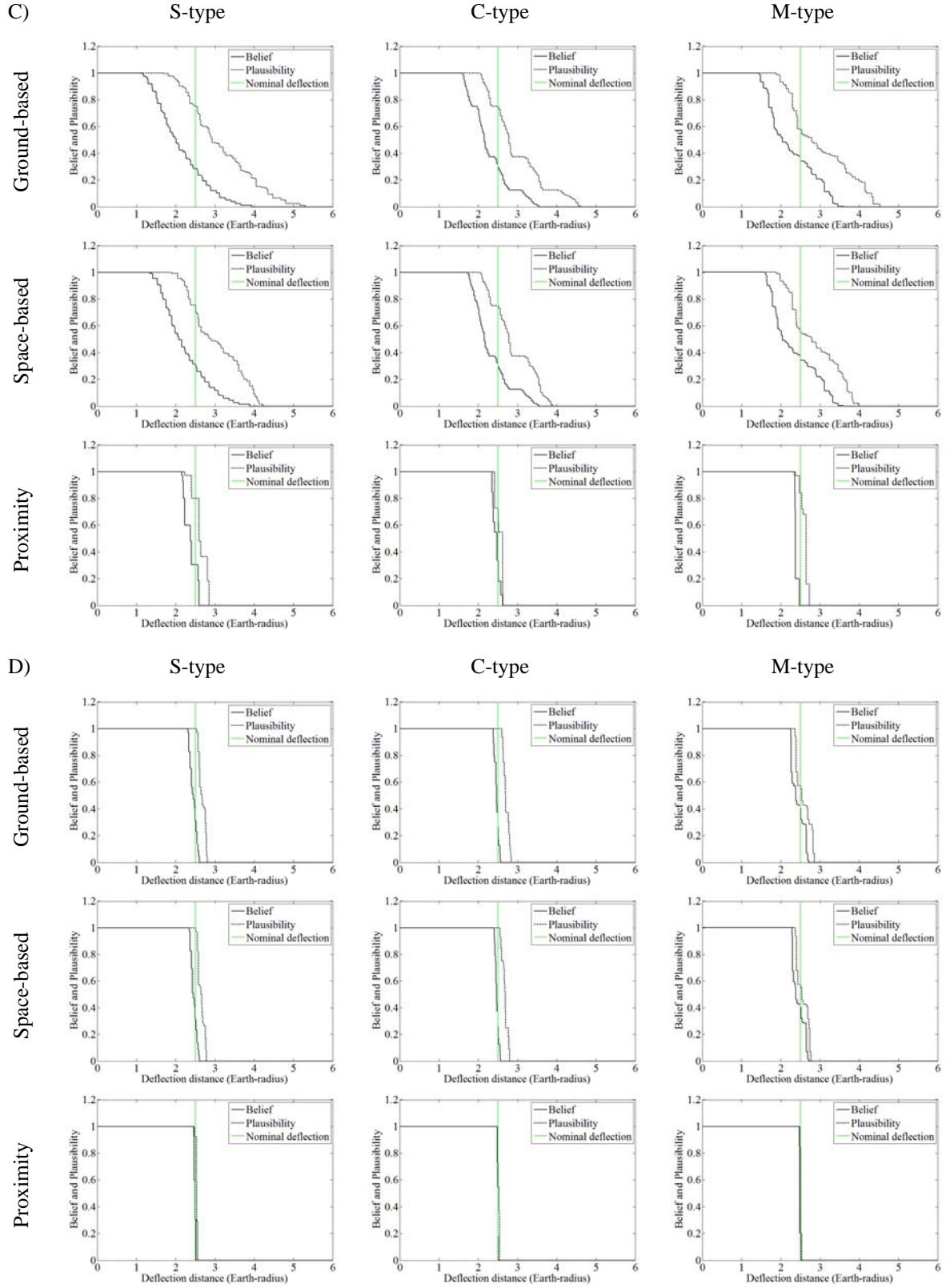
Figure 8 Belief and Plausibility of deflection on the 2036 b-plane for different characterisation scenarios and asteroid classes. Black lines represent Belief measures whereas dashed black lines represent Plausibility measures. Green lines represent the nominal deflection distance b_{nom}. C) SC. D) GT.

4. Mitigation campaign planning

Mitigation campaigns should be accurately planned in order to provide a successful deflection even if the preliminary NEA characterisation is incomplete. Sending multiple spacecraft/interceptors of one specific type of deflection technique (e.g. the multiple solar mirror concept of Maddock et al. [23] and the multiple GT concept of Foster et al. [24]) can increase the deflection efficiency as well as the redundancy of given deflection mission. However, such mitigation campaigns are inevitably subject to the uncertain performance of a specific deflection technique due to not only the epistemic uncertainties in the NEA characteristics but aleatory/practical uncertainties in the technique (e.g. the precision of a KI, the time-variable sublimation efficiency of a SC, etc.).

To overcome the limits imposed on hazardous NEA mitigation campaigns of a single type deflection mission and to make the campaigns more reliable and robust, this work focuses on mitigation campaigns consisting of primary and secondary deflection missions (i.e. dual-deflection campaigns). The primary deflection mission makes use of an instantaneous deflection technique whereas the secondary deflection mission makes use of a slow push deflection technique. The final outcome of a dual-deflection campaign is therefore determined by the secondary deflection mission which performs its slow-push interception according to the outcome of in-situ NEA characterisation conducted by itself and the instantaneous outcome of the primary interception that could be fully successful, partly successful, or at worst, a complete failure. The secondary deflection mission should also be capable of preventing the NEA from undesired keyhole passage on the 2036 b-plane due to the primary deflection mission in order to avoid a subsequent Earth impact.

4.1. Dual-deflection campaign

Dual-deflection campaigns studied here consist of a primary interceptor (KI) and a secondary interceptor (GT). Figure 9 represents an example of dual-deflection campaign consisting of a KI and a GT (i.e. KI-GT campaign). The transfer orbits are designed by solving a two-body Lambert's problem. A conventional chemical propulsion system of $Isp = 300$ sec is used as a kick stage at the Earth departure and to accelerate or decelerate at the final approach to the target NEA. For the case of KI-GT campaign, two interceptors are sent to the NEA separately and hence follow two different trajectories. This is due to the fact that the KI takes advantage of a higher relative velocity at the NEA encounter whereas the GT requires a smaller relative velocity at the NEA rendezvous in order to reduce the total amount of delta-v for the orbital transfers. For this reason, the GT arrival can be, in theory, earlier than the KI's arrival. In this case, we assume that the secondary interception (GT) can be operational before and after the primary interception (KI) takes place according to the outcome of proximity characterisation of the target NEA conducted by GT.

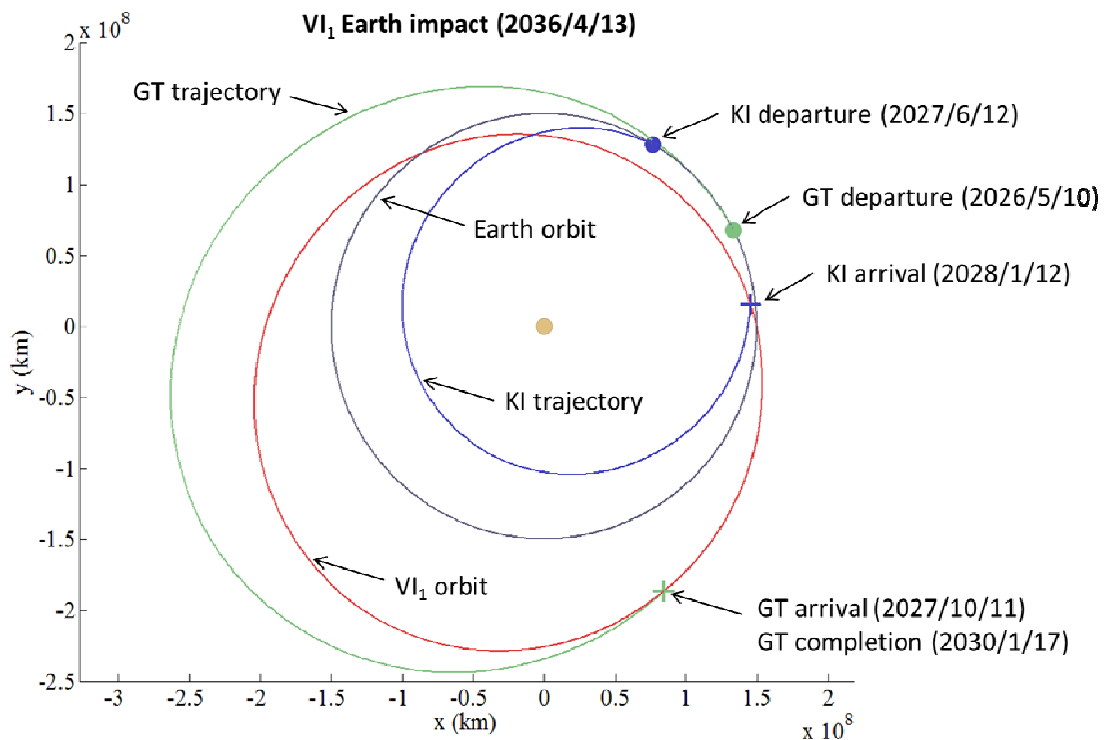Figure 9 Example of KI-GT campaign. The NEA orbit is represented in red. The transfer orbit of KI is represented in blue. The transfer orbit of GT is represented in green. Earth's orbit is represented in grey. The blue and green circles represent the Earth departure points of the KI and GT, respectively. The KI and GT rendezvous points with the NEA are represented as the blue and green cross shapes, respectively.

The minimum and maximum values of design variables $\mathbf{x}$ for a KI-GT campaign are given in Table 8. m_1 and m_2 are the masses of primary and secondary mitigation systems at the NEA arrival, respectively. t_1 and tof_1 are the Earth departure time and the flight time of the primary interceptor whereas t_2 and tof_2 are the Earth departure time and the flight time of the secondary interceptor. v_{imp} is the relative velocity component of the KI parallel to the flight direction of the NEA. t_{push} is the tractoring period of the GT.

Table 8 Minimum and maximum values of design variables $\mathbf{x}$ for a KI-GT campaign.

	m_1 (kg)	m_2 (kg)	t_1	tof_1 (day)	t_2	tof_2 (day)	v_{imp} (km/s)	t_{push} (day)
min	500	500	2026/4/13	100	2026/4/13	100	0	0
max	10000	20000	2033/7/11	1000	2033/7/11	1000	30	3650

4.2.   Campaign optimisation

In order to design a dual-deflection campaign, a number of trade-offs between competing aspects must be evaluated and optimised in order to minimise the launch cost and total campaign period while maximising the deflection performance and confidence level on mitigation campaign. The campaign optimisation problem requires evaluating the figures of merit (i.e. mitigation performance indicators $\mathbf{y}$) that characterise the performance and the confidence in successful mitigation campaign. The mitigation performance indicators $\mathbf{y}$ is given as

$$\mathbf{y} = \begin{bmatrix} m_0, & t_{f1}, & t_{f2}, & -b_{\mathrm{nom}}, & -Bel_{\mathrm{nom}} \end{bmatrix} \tag{16}$$

where five figures of merit that characterise the optimality of mitigation campaign are:

- m_0 is the total mass of two hazardous NEA mitigation systems at the Earth departure stage (EDS), which should be as small as possible to reduce the cost of the mitigation campaign.
- t_{f1} is the completion time of the primary deflection mission, which is desirable to be as early as possible such that a longer interception by the secondary deflection mission after the primary interception can be available. In addition, earlier completion of the primary interception is simply preferable for safety reasons.
- t_{f2} is the completion time of secondary deflection mission (i.e. campaign completion time), which should also be as early as possible such that an additional mitigation campaign can be launched, if necessary.
- b_{nom} is the nominal deflection on the b-plane, which is desired to be as large as possible within the range of $b_\oplus < b_{\mathrm{nom}} < b_{\mathrm{safe}}$.
- Bel_{nom} is Belief of nominal deflection, and thus higher Belief indicates higher confidence in successful mitigation.

The constraints on $\mathbf{y}$ are given as

$$\begin{bmatrix} m_0 \leq 200, & t_{f1} \leq t_{f2} \leq t_{\mathrm{MOID}}, & b_\oplus \leq b_{\mathrm{nom}} \leq b_{\mathrm{safe}}, & b_{\mathrm{trim}} \geq 1000 \end{bmatrix} \tag{17}$$

where m_0 is limited to 200 tons and t_{f1} can be no later than t_{f2} in order to allow the secondary interceptor to conduct a necessary trim manoeuvre for keyhole avoidance after the primary interception. The nominal deflection b_{nom} must be at least $b_\oplus$ and can be as large as b_{safe}. The deflection distance b_{trim} that can be provided by the trim manoeuvre of the secondary deflection mission by GT after the primary interception must be greater than 1000 km. This seems to be more than enough to avoid undesired keyhole passage due to the primary deflection mission according to the JPL report [5].

In this work, the fast and elitist multiobjective genetic algorithm NSGA-II proposed in the work of Deb et al. [25] is used to compute Pareto optimal design points of dual-deflection mitigation campaigns. A total of 2400 solutions for the mitigation performance indicators $\mathbf{y}$ are numerically computed in MATLAB.

5.   Results and discussion

The results of KI-GT campaigns against VI_1 of S-type asteroid characterised at the ground-based level are presented in Figure 10. The Pareto-optimal solutions for the campaigns are presented in terms of the campaign completion time (i.e. the completion time t_{f2} of the GT) and the total interceptor mass m_0 at the EDS, which are categorised into eight different levels of the Belief measure of nominal deflection; Bel_{nom}.

One of the notable aspects of dual-deflection campaigns is that Bel_{nom} is highly dependent on both total interceptor mass m_0 at the EDS and the campaign completion time t_{f2}. For the KI-GT campaign scenario, there are quite a few optimal KI-GT campaigns available within 100–150 tons of m_0, given $Bel_{\mathrm{nom}} \leq 0.57$ and 2–4

years of t_{f2}, whereas there are almost no KI-GT campaigns available within 100–150 tons of m_0, given $Bel_{nom} \geq 0.83$ and <4 years of t_{f2}.

Also, it can be seen that a longer campaign period (>6 years) does not necessarily increases the overall mitigation performance including Bel_{nom} but actually there are many optimal dual-deflection campaigns with a nominal deflection as large as 2.5 Earth-radii within 3–6 years of t_{f2} for $Bel_{nom} \geq 0.70$ without requiring a significantly large amount of total interceptor mass relative to that for longer-term campaigns. This appears to be simply due to the fact that later asteroid deflection missions are less efficient than earlier ones.

Table 9 shows a series of design variables $\mathbf{x}$ and mitigation performance indicators $\mathbf{y}$ for some examples of optimal KI-GT mitigation campaigns with different degrees of confidence in nominal deflection. Particularly for the KI-GT campaign scenario against VI$_1$, the GT rendezvous with the NEA approximately <2 years before or <1 year after the KI arrival/interception time depending on the respective KI-GT campaign sequences, where the former case is found to be highly beneficial in terms of the proximity characterisation of the NEA as well as of the precise guidance of the KI by GT. The GT might start tractoring immediately after the NEA rendezvous without waiting for the KI arrival/impact, however most importantly, this is not always the case particularly when the true values of the NEA physical properties are in the nominal conditions or much more favourable conditions (e.g. less heavy NEA mass than expected, smaller in size, etc.). If the in-situ NEA physical characteristics result in a favourable outcome, the GT will simply add an extra deflection to the outcome of the primary interception. It can also be seen that the avoidance of undesired keyhole passage due to the primary interception is fulfilled, counting on the reserved deflection b_{trim} by the GT trim manoeuvre after the primary interception. The period of time to achieve b_{trim} ranges from 107 days to 9.35 years.

Furthermore, the preliminary results of the KI-GT campaign scenario imply that not only the NEA arrival but the Earth departure of the KI could be even later than the GT arrival at the NEA, depending on the availability that is subject to the launch window, warning time, NEA orbit, etc. This would be beneficial for the mitigation system design of KI as a primary interceptor because the GT can conduct preliminary characterisation of the NEA at the proximity level in advance of the Earth departure of the KI, and thus investigating the availability of such a precursor characterisation mission by GT should be subject of future work.

Table 9 Design variables $\mathbf{x}$ and mitigaiton performance indicators $\mathbf{y}$ for some examples of optimal KI-GT mitigation campaigns with different degrees of Bel_{nom}. A) $Bel_{nom} \geq 0.47$. B) $Bel_{nom} \geq 0.56$. C) $Bel_{nom} \geq 0.70$. D) $Bel_{nom} \geq 0.83$. E) $Bel_{nom} \geq 0.97$. F) $Bel_{nom} = 1.00$.

| A)	m_1 (kg)	m_2 (kg)	t_1	tof_1 (day)	t_2	tof_2 (day)	v_{imp} (km/s)	t_{push} (day)
	2660	2734	2026/4/14	296	2026/5/12	536	12.5	746
	m_0 (ton)	t_{f1}	t_{f2}	b_{nom} (Earth-radius)		b_{trim} (km)	Bel_{nom}	Pl_{nom}
	72	2027/2/4	2029/11/14	2.26		1083	0.47	0.83
B)	m_1 (kg)	m_2 (kg)	t_1	tof_1 (day)	t_2	tof_2 (day)	v_{imp} (km/s)	t_{push} (day)
	2440	5813	2027/1/2	536	2026/5/14	558	16.3	801
	m_0 (ton)	t_{f1}	t_{f2}	b_{nom} (Earth-radius)		b_{trim} (km)	Bel_{nom}	Pl_{nom}
	99	2028/6/21	2030/1/31	2.36		1275	0.56	1.00
C)	m_1 (kg)	m_2 (kg)	t_1	tof_1 (day)	t_2	tof_2 (day)	v_{imp} (km/s)	t_{push} (day)
	7147	6948	2028/7/6	312	2026/5/7	563	5.56	1102
	m_0 (ton)	t_{f1}	t_{f2}	b_{nom} (Earth-radius)		b_{trim} (km)	Bel_{nom}	Pl_{nom}
	112	2029/5/14	2030/11/27	2.34		1085	0.70	1.00
D)	m_1 (kg)	m_2 (kg)	t_1	tof_1 (day)	t_2	tof_2 (day)	v_{imp} (km/s)	t_{push} (day)
	7150	6948	2028/7/6	312	2026/5/11	563	5.00	1102
	m_0 (ton)	t_{f1}	t_{f2}	b_{nom} (Earth-radius)		b_{trim} (km)	Bel_{nom}	Pl_{nom}
	113	2029/5/14	2030/12/1	2.08		1097	0.83	1.00
E)	m_1 (kg)	m_2 (kg)	t_1	tof_1 (day)	t_2	tof_2 (day)	v_{imp} (km/s)	t_{push} (day)
	6593	8745	2028/6/4	356	2026/5/6	551	6.05	1330
	m_0 (ton)	t_{f1}	t_{f2}	b_{nom} (Earth-radius)		b_{trim} (km)	Bel_{nom}	Pl_{nom}
	143	2029/5/26	2031/6/30	2.47		1708	0.97	1.00
F)	m_1 (kg)	m_2 (kg)	t_1	tof_1 (day)	t_2	tof_2 (day)	v_{imp} (km/s)	t_{push} (day)
	7302	10736	2028/6/21	322	2026/5/10	556	5.71	1009
	m_0 (ton)	t_{f1}	t_{f2}	b_{nom} (Earth-radius)		b_{trim} (km)	Bel_{nom}	Pl_{nom}
	166	2029/5/9	2030/8/22	2.42		1417	1.00	1.00
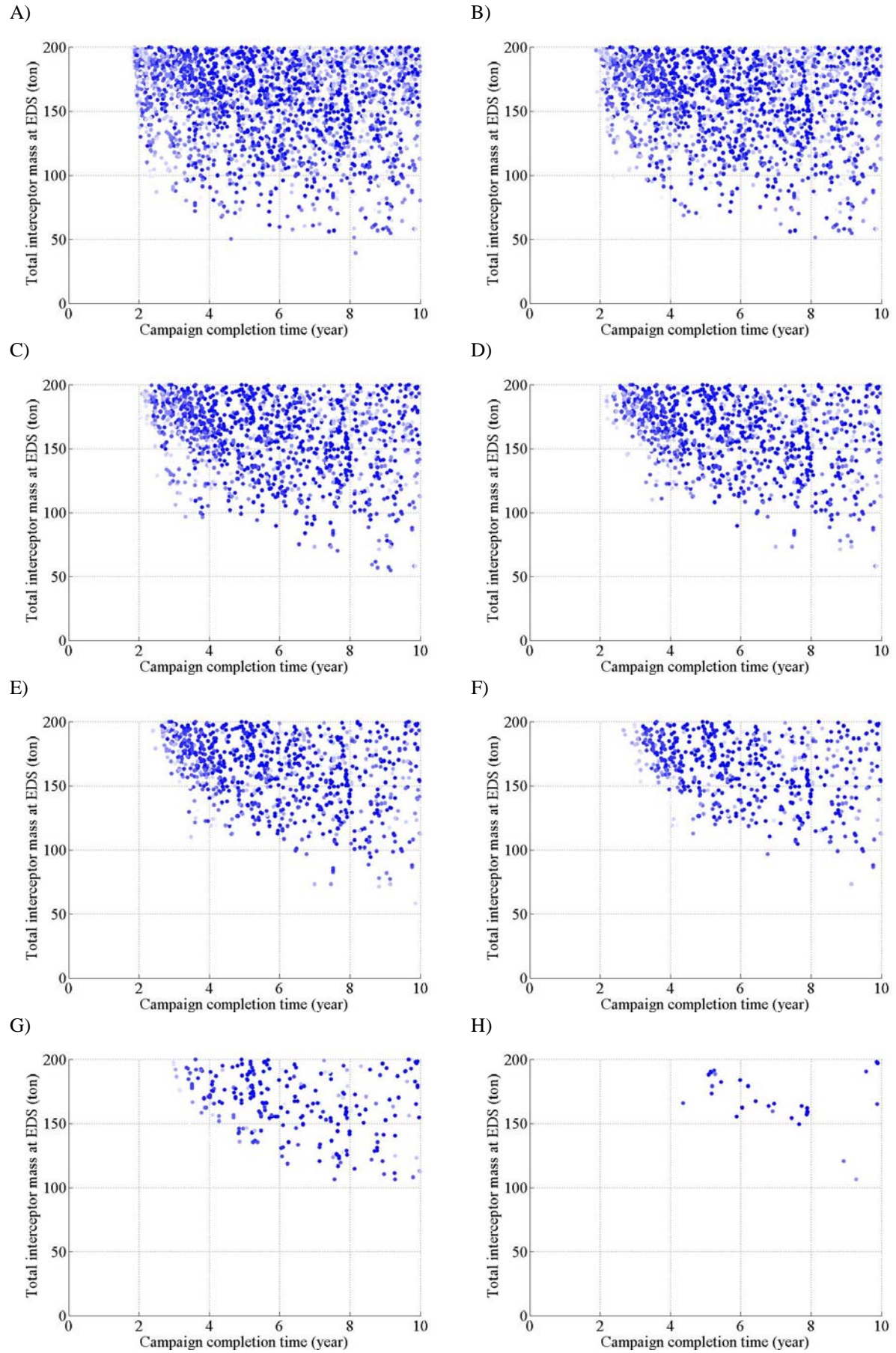
Figure 10 Optimal solutions for KI-GT campaigns. Deeper blue dots represent higher values of b_{nom} whereas fainter blue dots represent lower values of b_{nom}. A) $Bel_{\text{nom}} \geq 0.47$. B) $Bel_{\text{nom}} \geq 0.51$. C) $Bel_{\text{nom}} \geq 0.56$. D) $Bel_{\text{nom}} \geq 0.57$. E) $Bel_{\text{nom}} \geq 0.70$. F) $Bel_{\text{nom}} \geq 0.83$. G) $Bel_{\text{nom}} \geq 0.97$. H) $Bel_{\text{nom}} = 1.00$.

Conclusions

A hazardous NEA mitigation campaign planning based on uncertain information on the fundamental asteroid characteristics has been studied to improve the mitigation campaign credibility, where one of the possible forms of mitigation campaign – dual-deflection campaign – has been investigated in detail. In order to evaluate the confidence level on deflection missions subject to the uncertain NEA characteristics, the uncertainty quantification technique called Evidence Theory is used. The preliminary results of the dual-deflection campaigns consisting of a primary KI and a secondary GT have shown that:

- Dual-deflection campaign planning involves a series of competing aspects that must be assessed and constraints associated with the specific configurations of KI-GT to be satisfied to plan a mitigation campaign with sufficient performance (i.e. deflection) and high confidence in successful deflection (i.e. Belief).
- Given a GT as a secondary deflection mission, Belief of nominal deflection can be improved by years of GT interception manoeuvre before and after a primary deflection mission for the KI-GT campaign scenario. However, this does not necessarily means that the GT must always commence its interception immediately after the NEA rendezvous but the actual operation of the GT is subject to the in-situ NEA characteristics.
- Given a 10-year warning time, a mitigation campaign with a completion time of approximately half the warning time seems to be more reasonable than a longer-term mitigation campaign or a mitigation campaign with a heavier total interceptor mass at the EDS. In other words, this appears to be due to the deflection performance decrease with time and increase in the launch cost of necessary mitigation systems for a shorter-term mitigation campaign.
- Possible keyhole passage due to undesired deflection by a primary interception can be avoided by a GT as a secondary deflection mission in a dual-deflection campaign given the necessary amount of deflection in order to avoid the keyhole passage is 1000km.

Finally, the particular campaign planning approach presented here could be useful for the near-future hazard mitigation campaigns where we might have to tap into our incomplete knowledge on NEAs for mitigation campaign design, allowing us to select the best possible combination of deflection missions from a catalogue of various possible mitigation campaign options, without compromising the campaign credibility. However in the foreseeable future, further knowledge about the NEA population and some specific NEAs will have steadily accumulated and improved through the forthcoming NEA survey and exploration missions such as NEOSSat, Sentinel, Hayabusa2, and OSIRIS-Rex as well as the recently announced NASA's NEA retrieval mission to be launched as soon as the year 2017.

Appendices

A.1.   BPA structures for NEA physical properties

The uncertain NEA physical properties, more specifically, micro density ρ_{micro}, micro porosity P_{micro}, bulk porosity P_{bulk}, and albedo p_v are represented in the forms of BPA structures (i.e. a set of interval values with prescribed BPAs), respectively. The BPA structures for the S-type, C-type, and M-type NEAs are given in Table 10. Also, three different characterisation scenarios (the ground-based, space-based, and proximity-based characterisation scenarios) are taken into consideration, where differences in three uncertainty levels are represented appropriately by scaling down the overall interval of any parameter which is eligible to be more certain and by referring to the capability and limits of respective characterisation scenarios. The following sub-subsections present the details on the formation of the BPA structures for the respective taxonomic classes and the characterisation scenarios, acknowledging all the corresponding supporting information regarding these NEA physical properties.

A.1.1. S-type

The meteorite analogues of S-type asteroids were believed to be stony meteorites even before the Hayabusa spacecraft visited the S-type asteroid, namely 25143 Itokawa. The Hayabusa mission finally confirmed directly that the characteristics of Itokawa's surface grains returned by the Hayabusa spacecraft are consistent with the characteristics of L, LL, and partly H chondrites [26]. Most importantly, the Hayabusa mission has proved the analogy between meteorites and NEA compositions through the in-situ study of the asteroid for the first time.

The microscopic physical parameters of S-type asteroids are often estimated by referring to their meteorite analogues – ordinary chondrites (OCs), assuming they are homogeneously composed of OCs, L, LL, and H chondrites in particular. Although, the Hayabusa mission revealed that Itokawa's surface is mostly made of L and LL chondrites [27], we cannot rule out the possible presence of subsurface metal-rich particles such as H chondrites buried inside Itokawa due to successive impact events.

BPA structures for the physical properties of S-type asteroids are given in Table 10. The BPA structures for the micro density ρ_{micro} are formed by referring to 437 samples of H, L, and LL chondrites [28]. In order to form the BPA structures for the micro porosity P_{micro}, micro porosities of 691 OCs [29] are referred and aggregated with additional data on micro porosities of 291 OCs from the different literature [30] by Dempster's rule of combination [21]. While most meteorites found on Earth spent long periods of time on the ground, and thus they are affected by considerable terrestrial weathering, it is noteworthy that the literature referred for P_{micro} of OCs used in this study is de-biased to such effects. This is due to the fact that the majority of meteorite falls are stony meteorites and about 80% of which are OCs, hence the amount of information on non-weathered OCs is consequently most abundant among our collection of meteorite collection.

The abundance of S-type asteroids amongst the well-characterised asteroids [14] and the series of exploration missions to the S-type asteroids also results in better understanding of the macroscopic characteristics of S-type asteroids. The BPA structures for the bulk porosity P_{bulk} of S-type asteroids are formed by referring to the bulk porosities of 7 existing S-type asteroids (smaller than 100 km in diameter) with bulk porosities ranging 20–60% [14]. Finally, the BPA structures for the albedo p_v are formed by referring to the observed geometric albedos of 30 different S-type asteroids [31].

A.1.2. C-type

The microscopic physical parameters of C-type asteroids can be roughly estimated by referring to their meteorite analogues – carbonaceous chondrites (CCs), assuming they are homogeneously composed of CCs. Since CCs represent less than 5% of stony meteorite falls, the information on non-weathered CCs is limited.

BPA structures for the physical properties of C-type asteroids are given in Table 10. The BPA structures for the micro density ρ_{micro} is formed by referring to 11 CM chondrites [32]. The micro porosity P_{micro} is simply assumed to be 15.5–30.5% [28] which is consistent with the work of Flynn et al. [33]. This simple assumption is mainly due to the insufficient amount of sample data for non-biased micro porosities of CCs.

C-type asteroids are second most abundant amongst the discovered NEAs, however unlike S-type asteroids, in-situ exploration missions to C-type asteroids (e.g. Hayabusa 2 and OSIRIS-REx) are yet to be sent, and hence the macroscopic characteristics of C-type asteroids are highly unknown. The BPA structures for the bulk porosity P_{bulk} of C-type asteroids are formed by referring to 8 existing C-type asteroids of various sizes with bulk porosities ranging 30–70% [14]. Finally, the BPA structures for the albedo p_v are formed by referring to the observed geometric albedos of 18 different C-type asteroids [31].

Some of the discovered M-type asteroids (e.g. 21 Lutetia, 22 Kalliope, 129 Antigone, and 785 Zwetana) are not entirely consistent with typical iron-nickel meteorite analogues whereas (e.g. 16 Psyche, 216 Klepatra, and (6178) 1986 DA) appear to be metallic. One of the smallest M-type asteroids, namely (6178) 1986 DA is a very good candidate of metallic asteroids which are thought to be a remnant of the core of a fractured primitive body from the early solar system. The meteorite analogues of metallic M-type asteroids are basically iron meteorites.

A.1.3. M-type

The microscopic physical parameters of M-type asteroids can be roughly estimated by referring to their meteorite analogues – iron meteorites, assuming they are homogeneously composed of iron meteorites. Iron meteorites represent less than 6% [34] of all the meteorite falls, and thus the amount of information on non-weathered iron meteorites is most limited.

Iron meteorites are known to be more immune to terrestrial weathering, and thus there is usually less difference between weathered and unweathered samples than fragile chondrite meteorites. BPA structures for the physical properties of M-type asteroids are given in Table 10. The BPA structures for the micro density ρ_{micro} is formed by referring to 21 iron-nickel meteorites [35]. The micro porosity P_{micro} is simply assumed to be 0–1.2% [36]. This range is consistent with the iron-nickel meteorites of the Vatican collection with porosities of near zero [37].

M-type asteroids are least abundant amongst the three asteroid types, and thus their macroscopic characteristics are mostly unknown. Not to mention, they have not been characterised by spacecraft and, unlike S-type and C-type asteroids, remote characterisation of M-type asteroids is not an easy task because the spectrum analysis of them provide us with less information than that of the other two types does. The BPA structures for the bulk porosity P_{bulk} of M-type asteroids are formed by referring to 7 existing M-type asteroids of various sizes with bulk porosities ranging 0–40% [14]. Finally, the BPA structures for the albedo p_v are formed by referring to the observed geometric albedo of 10 different M-type asteroids [31].

Table 10 BPA structures for the NEA physical properties of S-type, C-type, and M-type asteroids. A) Ground-based characterisation. B) Space-based characterisation. C) Proximity characterisation.

A)	S-type		C-type		M-type	
	Interval	BPA	Interval	BPA	Interval	BPA
ρ_{micro} (g/cm^3)	[3.23, 3.30]	0.31	[2.57, 2.60]	0.18	[7.59, 7.60]	0.05
	[3.30, 3.50]	0.29	[2.60, 2.70]	0.36	[7.60, 7.80]	0.19
	[3.50, 3.70]	0.33	[2.70, 2.80]	0.18	[7.80, 8.00]	0.62
	[3.70, 3.84]	0.07	[2.80, 2.86]	0.27	[8.00, 8.07]	0.14
P_{micro} (%)	[3.7, 5.0]	0.01	[15.5, 30.5]	1.00	[0.0, 1.2]	1.00
	[5.0, 7.5]	0.10				
	[7.5, 10.0]	0.30				
	[10.0, 12.5]	0.32				
	[12.5, 15.0]	0.22				
	[15.0, 16.3]	0.05				
P_{bulk} (%)	[16.4, 30.0]	0.43	[27.5, 40.0]	0.25	[0.0, 10.0]	0.43
	[30.0, 40.0]	0.14	[40.0, 50.0]	0.37	[10.0, 20.0]	0.14
	[40.0, 50.0]	0.29	[50.0, 60.0]	0.25	[20.0, 30.0]	0.14
	[50.0, 56.0]	0.14	[60.0, 67.8]	0.13	[30.0, 37.9]	0.29
p_v	[0.10, 0.15]	0.27	[0.04, 0.05]	0.33	[0.08, 0.11]	0.30
	[0.15, 0.20]	0.37	[0.05, 0.06]	0.44	[0.11, 0.13]	0.40
	[0.20, 0.25]	0.23	[0.06, 0.07]	0.17	[0.13, 0.16]	0.10
	[0.25, 0.28]	0.13	[0.07, 0.073]	0.06	[0.16, 0.17]	0.20

B)	S-type		C-type		M-type	
	Interval	BPA	Interval	BPA	Interval	BPA
ρ_{micro} (g/cm^3)	[3.23, 3.30]	0.31	[2.57, 2.60]	0.18	[7.59, 7.60]	0.05
	[3.30, 3.50]	0.29	[2.60, 2.70]	0.36	[7.60, 7.80]	0.19
	[3.50, 3.70]	0.33	[2.70, 2.80]	0.18	[7.80, 8.00]	0.62
	[3.70, 3.84]	0.07	[2.80, 2.86]	0.27	[8.00, 8.07]	0.14
P_{micro} (%)	[3.7, 5.0]	0.01	[15.5, 30.5]	1.00	[0.0, 1.2]	1.00
	[5.0, 7.5]	0.10				
	[7.5, 10.0]	0.30				
	[10.0, 12.5]	0.32				
	[12.5, 15.0]	0.22				
	[15.0, 16.3]	0.05				
P_{bulk} (%)	[21.4, 30.0]	0.43	[32.5, 40.0]	0.25	[2.86, 10.0]	0.43
	[30.0, 40.0]	0.14	[40.0, 50.0]	0.37	[10.0, 20.0]	0.14
	[40.0, 50.0]	0.29	[50.0, 60.0]	0.25	[20.0, 30.0]	0.14
	[50.0, 51.4]	0.14	[60.0, 62.5]	0.13	[30.0, 32.9]	0.29
p_v	[0.14, 0.15]	0.31	[0.041, 0.05]	0.33	[0.09, 0.11]	0.30
	[0.15, 0.20]	0.42	[0.05, 0.06]	0.44	[0.11, 0.13]	0.40
	[0.20, 0.25]	0.27	[0.06, 0.07]	0.17	[0.13, 0.15]	0.10
			[0.07, 0.071]	0.06	[0.15, 0.16]	0.20

C)	S-type		C-type		M-type	
	Interval	BPA	Interval	BPA	Interval	BPA
ρ_{micro} (g/cm^3)	[3.26, 3.30]	0.31	[2.59, 2.60]	0.18	[7.64, 7.80]	0.20
	[3.30, 3.50]	0.29	[2.60, 2.70]	0.36	[7.80, 8.00]	0.65
	[3.50, 3.70]	0.33	[2.70, 2.80]	0.18	[8.00, 8.04]	0.15
	[3.70, 3.76]	0.07	[2.80, 2.83]	0.27		
P_{micro} (%)	[8.2, 10.0]	0.35	[19.8, 26.3]	1.00	[0.0, 1.2]	1.00
	[10.0, 12.5]	0.39				
	[12.5, 13.2]	0.26				
P_{bulk} (%)	[34.4, 34.4]	1.00	[45.7, 45.7]	1.00	[13.1, 13.1]	1.00
p_v	[0.17, 0.20]	0.61	[0.049, 0.05]	0.43	[0.11, 0.13]	0.80
	[0.20, 0.21]	0.39	[0.05, 0.06]	0.57	[0.13, 0.131]	0.20

References

[1] J.P. Sanchez, C. Colombo, M. Vasile, G. Radice, Multicriteria Comparison Among Several Mitigation Strategies for Dangerous Near-Earth Objects, Journal of Guidance, Control, and Dynamics, 32 (2009) 121-142.

[2] Defending Planet Earth: Near-Earth Object Surveys and Hazard Mitigation Strategies: Final Report, in, Committee to Review Near-Earth Object Surveys and Hazard Mitigation Strategies; National Research Council, 2010.

[3] Y. Sugimoto, G. Radice, J.P. Sanchez, Effects of NEO composition on deflection methodologies, Acta Astronautica, in press (2012) DOI:10.1016/j.actaastro.2012.1008.1030.

[4] A. Milani, S.R. Chesley, P.W. Chodas, G.B. Valsecchi, Asteroid Close Approaches: Analysis and Potential Impact Detection, in: W.F. Bottke Jr., A. Cellino, P. Paolicchi, R.P. Binzel (Eds.) Asteroids III, University of Arizona Press, Tucson, 2002, pp. 55-69.

[5] Near-Earth Object (NEO) analysis of transponder tracking and gravity tractor performance, in, JPL Task Plan No. 82-120022, 2008.

[6] A.W. Harris, M.A. Barucci, J.L. Cano, A. Fitzsimmons, M. Fulchignoni, S.F. Green, D. Hestroffer, V. Lappas, W. Lork, P. Michel, D. Morrison, D. Payson, F. Schaefer, A global approach to near-Earth object impact threat mitigation, in: 2011 IAA Planetary Defense Conference, International Academy of Astronautics, Bucharest, 2011.

[7] S. Hasegawa, T.G. Müller, K. Kawakami, T. Kasuga, T. Wada, Y. Ita, N. Takato, H. Terada, T. Fujiyoshi, M. Abe, Albedo, Size, and Surface Characteristics of Hayabusa-2 Sample-Return Target 162173 1999 JU3 from AKARI and Subaru Observations, Publications of the Astronomical Society of Japan, 60 (2008) S399-S405.

[8] R.B. Adams, J.W. Campbell, R.C. Hopkins, W.S. Smith, W. Arnold, J. Sverdrup, M. Baysinger, T. Crane, P. Capizzo, S. Sutherlin, J. Dankanich, G. Woodcock, G. Edlin, J. Rushing, L. Fabisinski, D. Jones, S. McKamey, S. Thomas, C. Maccone, G. Matloff, J. Remo, Near Earth Object (NEO) Mitigation Options Using Exploration Technologies, in: Planetary Defense Conference, Washington, DC, 2007.

[9] P. Michel, Physical properties of Near-Earth Objects that inform mitigation, Acta Astronautica, (2012) DOI:10.1016/j.actaastro.2012.1007.1022.

[10] T.G. Müller, T. Sekiguchi, M. Kaasalainen, M. Abe, S. Hasegawa, Itokawa: The power of ground-based mid-infrared observations, in: A. Milani, G.B. Valsecchi, D. Vokrouhlický (Eds.) Proceedings of the International Astronomical Union Symposium, Cambridge University Press, 2006, pp. 261-266.

[11] F. Zuiani, M. Vasile, A. Gibbings, Evidence-Based Robust Design of Deflection Actions for Near Earth Objects, Celestial Mechanics and Dynamical Astronomy, 114 (2012) 107-136.

[12] R.R. Yager, M. Federizzi, J. Kacprzyk, Advances in the Dempster-Shafer Theory of Evidence, John Wiley & Sons Inc., Hoboken, 1994.

[13] S. Abe, T. Mukai, N. Hirata, O.S. Barnouin-Jha, A.F. Cheng, H. Demura, R.W. Gaskell, T. Hashimoto, K. Hiraoka, T. Honda, T. Kubota, M. Matsuoka, T. Mizuno, R. Nakamura, D.J. Scheeres, M. Yoshikawa, Mass and Local Topography Measurements of Itokawa by Hayabusa, Science, 312 (2006) 1344.

[14] J. Baer, S.R. Chesley, R.D. Matson, Astrometric masses of 26 asteroids and observations on asteroid porosity, The Astronomical Journal, 141 (2011) 143-155.

[15] M. Vasile, C. Colombo, Optimal impact strategies for asteroid deflection, Journal of Guidance, Control, and Dynamics, 31 (2008) 858-872.

[16] J.P. Sanchez, C. Colombo, Impact Hazard Protection Efficiency by a Small Kinetic Impactor, Journal of Spacecraft and Rockets, in press (2012) DOI:10.2514/2511.A32304.

[17] E.J. Öpik, Collision probabilities with the planets and the distribution of interplanetary matter, Proceedings of the Royal Irish Academy. Section A: Mathematical and Physical Sciences, 54 (1951) 165-199.

[18] W.F. Bottke Jr., A. Morbidelli, Debiased Orbital and Absolute Magnitude Distribution of the Near-Earth Objects, Icarus, 156 (2002) 399-433.

[19] Sentinel Mission, in, B612 Foundation, 2012.

[20] D. Morrison, C.R. Chapman, D. Steel, R.P. Binzel, Impacts and the public: communicating the nature of the impact hazard, in: M.J.S. Belton, T.H. Morgan, N.H. Samarasinha, D.K. Yeomans (Eds.) Mitigation of Hazardous Comets and Asteroids, Cambridge University Press, Cambridge, 2004, pp. 353-390.

[21] H. Agarwal, J.E. Renaud, E.L. Preston, Trust region managed reliability based design optimization using Evidence Theory, in: 44th AIAA/ASME/ASCE/AHS Structures, Structural Dynamics, and Materials Conference, Norfolk, 2003.

[22] K.A. Holsapple, K.R. Housen, Momentum transfer in asteroid impacts. I. Theory and scaling, Icarus, 221 (2012) 875-887.

[23] C.A. Maddock, J.P. Sanchez, M. Vasile, G. Radice, Comparison of Single and MultiSpacecraft Configurations of NEA deflection by Solar Sublimation, AIP conference Proceedings, 886 (2007) 303-316.

[24] C. Foster, J. Bellerose, D. Mauro, B. Jaroux, Mission concepts and operations for asteroid mitigation involving multiple gravity tractors, Acta Astronautica, (2012) DOI:10.1016/j.actaastro.2012.1010.1010.

[25] K. Deb, A. Pratap, S. Agarwal, T. Meyarivan, A Fast and Elitist Multiobjective Genetic Algorithm: NSGA-II, IEEE Transactions on Evolutionary Computation, 6 (2002) 182-197.

[26] M. Yoshikawa, A. Fujiwara, J. Kawaguchi, Hayabusa Mission & Science Team, The nature of asteroid Itokawa revealed by Hayabusa, in: A. Milani, G.B. Valsecchi, D. Vokrouhlický (Eds.) Proceedings of the International Astronomical Union Symposium, Cambridge University Press, 2006, pp. 401-416.

[27] H. Yurimoto, K. Abe, M. Abe, M. Ebihara, A. Fujimura, M. Hashiguchi, K. Hashizume, T.R. Ireland, S. Itoh, J. Katayama, C. Kato, J. Kawaguchi, N. Kawasaki, F. Kitajima, S. Kobayashi, T. Meike, T. Mukai, K. Nagao, T. Nakamura, H. Naraoka, T. Noguchi, R. Okazaki, C. Park, N. Sakamoto, Y. Seto, M. Takei, A. Tsuchiyama, M. Uesugi, S. Wakaki, T. Yada, K. Yamamoto, M. Yoshikawa, M.E. Zolensky, Oxygen Isotopic Compositions of Asteroidal Materials Returned from Itokawa by the Hayabusa Mission, Science, 333 (2011) 1116-1119.

[28] D.T. Britt, G.J. Consolmagno S.J., Stony meteorite porosities and densities: A review of the data through 2001, Meteoritics & Planetary Science, 38 (2003) 1161-1180.

[29] D.T. Britt, G.J. Consolmagno, Meteorite porosities and densities: A review of trends in the data, in: 35th Lunar and Planetary Science Conference, Houston, 2004.

[30] D.T. Britt, D. Yeomans, K. Housen, G. Consolmagno, Asteroid Density, Porosity, and Structure, in: W.F. Bottke Jr., A. Cellino, P. Paolicchi, R.P. Binzel (Eds.) Asteroids III, University of Arizona Press, Tucson, 2002, pp. 485-500.

[31] A.W. Harris, The H-G asteroid magnitude system: Mean slope parameters, Abstracts of the Lunar and Planetary Science Conference, 20 (1989) 375.

[32] B. Mason, The carbonaceous chondrites, Space Science Reviews, 1 (1962) 621-646.

[33] G.J. Flynn, L.B. Moore, W. Klöck, Density and Porosity of Stone Meteorites: Implications for the Density, Porosity, Cratering, and Collisional Disruption of Asteroids, Icarus, 142 (1999) 97-105.

[34] J.A. Wood, Meteorites and the Origin of Planets, McGraw-Hill Book Company, New York, 1968.

[35] E.P. Henderson, S.H. Perry, A discussion of the densities of iron meteorites, 1954, 6 (1954) 221-240.

[36] C.P. Opeil, G.J. Consolmagno, D.T. Britt, The thermal conductivity of meteorites: New measurements and analysis, Icarus, 208 (2010) 449-454.

[37] G.J. Consolmagno S.J., D.T. Britt, The density and porosity of meteorites from the Vatican collection, Meteoritics & Planetary Science, 33 (1998) 1231-1241.